International Journal of Multiphase Flow 105 (2018) 102–111

Contents lists available at ScienceDirect

International Journal of Multiphase Flow

journal homepage: www.elsevier.com/locate/ijmulflow

Transient modeling of one-dimensional solid-liquid flow in conduits

Ulf Jakob F. Aarsnes[a,*], Alexander Busch[b]

[a] International Research Institute of Stavanger (IRIS), Oslo, Norway
[b] Norwegian University of Science and Technology (NTNU), Trondheim, Norway

ARTICLE INFO

Article history:
Received 24 October 2017
Revised 26 March 2018
Accepted 31 March 2018
Available online 5 April 2018

Keywords:
Particle transport
PDE
Real-Time
Drilling
Cuttings transport
Layer model

ABSTRACT

We consider the transient modeling of liquid-solid flow in conduits. Current models available in the literature are typically based on a three layer – two phase representation which, for the general transient case, results in a six-field model, entailing significant complexity in analysis and implementation. In this paper, we propose a transient three layer model represented by three equations (a third order PDE) by assuming a static momentum balance and then exploiting certain properties of the continuity relations. We illustrate how the transient model can be completed by introducing deposition–erosion closure relations from the literature, and describe its implementation by an upwind numerical scheme. Finally, some of the transient properties of the model are illustrated in six simulations comparing the simulated trends with six cuttings transport experiments found in the literature, motivated by application to horizontal drilling.

1. Introduction

Solid-liquid flow in pipes and other conduits, for instance annuli and channels, find numerous applications such as slurry flows in waste handling, sediment transport in hydrology, and cuttings (drilled-off particles) transport in drilling (Tomren et al., 1986; Larsen et al., 1997; Philip et al., 1998). Here, transient cuttings transport models can improve drilling operations by optimizing transient procedures such as connections and back-reaming, and may be utilized as Real-Time (RT) models on the drill rig to provide on-line monitoring of hole cleaning (adequate flushing of cuttings from the wellbore) (Florence and Iversen, 2010). An overview of cuttings transport modeling is given by Pilehvari et al. (1999), and more recently, by Li and Luft (2014), while more general reviews of two-phase, solid-liquid flows are for instance given by Drew (1983) and Peker and Helvaci (2008).

Inherently, cuttings transport is a transient, spatial three-dimensional (3D) problem because the conduit is an annulus, where the inner drill pipe may be off-center (or even laterally moving) and rotating, and where a bed of cuttings may form at the lower wall in inclined and horizontal sections. For lower inclinations this bed is typically stationary but features a small layer of sliding and rolling particles (referred to as *bed load* in environmental particle transport modeling and hydrology) between the usually stationary bed and the bulk of the fluid-solid flow. However, for most simulation purposes, resolving the full 3D flow field may be too cumbersome, due to the complex interaction between the phases. In particular, calculating the temporal evolution of the interface between the phases, and the transfer momentum across it, may be too computationally costly, especially when Real-Time (RT) application of the model is desired. While 3D Computational Fluid Dynamics (CFD) methodologies have been used to investigate specific cuttings transport problems and further understand the interdependencies of parameters in and on the 3D flow field, todays available computational power limits 3D CFD approaches to a scale of the order of 10^0 m, whereas the wellbore scale is of the order of 10^3 m. As such, the full 3D CFD simulations are relegated to enhancing experimental work in deriving models for closure relations (such as slip velocities as well as deposition and entrainment rates) (Kaushal et al., 2012; Capecelatro and Desjardins, 2013; Busch et al., 2017), rather than providing RT models in themselves. In any case, for fast-computing requirements on the wellbore scale such as previously mentioned RT applications, a 3D formulation of the multiphase flow problem is to be simplified using local equilibrium assumptions and a complete spatial average over the cross-sectional area, leaving only the flow direction as a spatial dimension. The resulting coarse-grained one-dimensional in space (1D) models may still feature (relatively) high complexity depending on the number of phases considered and closures utilized.

Typically, 1D solid transport models in conduits are based on a two- or three layer formulation introduced by Doron and Barnea (1993), Doron and Barnea (1996) and Doron et al. (1997),

* Corresponding author.
E-mail addresses: ujfa@iris.no (U.J.F. Aarsnes), alexander.busch@alumni.ntnu.no (A. Busch).

https://doi.org/10.1016/j.ijmultiphaseflow.2018.03.023
0301-9322/

where the layers describe the above mentioned (stationary) bed, the (moving, in the sense of rolling and sliding particles) bed load and the flowing mixture of the transporting liquid with solids in suspension. Usually, balance equations are solved for mass and momentum for the solid and fluid phases in the individual layers. However, many models based on the layered approach are steady-state models, i.e. disregarding the transient terms.

Various transient 1D cuttings transport models have been proposed in the literature (Martins et al., 1998; Doan et al., 2003; Ramadan et al., 2005; Salazar-Mendoza and Espinosa-Paredes, 2009; Wang et al., 2010; Cayeux et al., 2014; Zhang et al., 2016) and have been shown capable of delivering significant value in field applications (Cayeux et al., 2016; Naganawa et al., 2017).

The closures utilized in these models may encompass comparatively simple single-phase *Reynolds number-friction factor*-relationships, slip velocity models (Chien, 1994), empirical correlations accounting for inclination, drill pipe rotation, or eccentricity (Larsen, 1990) and even numerical solutions of the cross-sectional flow field in order to capture secondary flows as a consequence of the solids bed (Girolami et al., 2016).

Existing transient 1D models are, however, relatively complicated and cumbersome to implement and analyze, and this complexity can limit the range of possible applications of the models, in particular with regards to model based estimation techniques (Aarsnes et al., 2016b). In addition, simplified mechanistic 1D models with semi-implicit or explicit solvers and closures are required to satisfy computational speed requirements (Florence and Iversen, 2010).

Based on these considerations, the present paper proposes a simple, phenomenological, modeling approach where considerations on time-scales and dominating dynamics are leveraged into formulating the complete model as a system of two or three hyperbolic equations, depending on the number of solid-liquid layers considered, completed by closure relations giving the suspended cuttings slip velocity as well as settling and erosion rates of the cuttings bed interface. The closure relations of the resulting model can be fitted to existing steady-state correlations to inherit the steady-state accuracy of previously published results, of which there are many (Tomren et al., 1986; Li and Walker, 2001). As such, the goal of the present paper is to provide a transient 1D simulation model, to enhance the applicability of existing steady-state results to cases where a RT-model is required. I.e., with this paper we wish to bridge this gap by providing a framework to make a steady-state model, or experimentally developed closure relations, into a transient simulation model, similarly to what was done with the Drift Flux Model in the 70's for liquid-gas flow.

Towards this goal, our hypothesis is that, firstly, a low order transient model (a PDE with two or three states) is sufficient to represent the transient dynamics on the time scale of the cuttings transportation. And, secondly, using steady-state flow closure relations from the literature, a transient model can be obtained without having to re-derive such closure relations specifically for the transient case.

To address this hypothesis, we give some general considerations on the continuity relations in Section 2, where under the assumption that the hydrodynamic time scale is much faster than that of the change of the bed height, the continuity of the six fields can be represented by three equations. Then, to illustrate the merit of this approach, transient simulations are performed and compared with experimental testing from cuttings transport in petroleum research where the model is shown to give a good qualitative representation of the dynamic behavior seen in experiments.

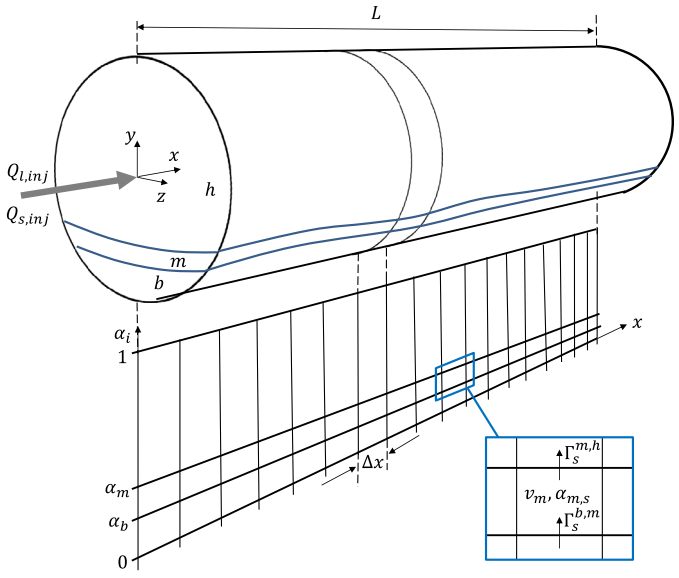

Fig. 1. Schematic of the three-layered model.

2. Starting point model

Consider a 3D field over the independent space variables *x, y, z*, and time, $t \in \mathbb{R}^+$. We denote by α_i, ρ_i, v_i the averaged volume fraction, density and velocity over a computational control volume, covering the *y, z* directions and with the infinitesimal small axial length Δx, schematically depicted in Fig. 1. Assuming the phase density ρ_i as constant, the continuity and momentum preservation equations (averaged over a computational control volume) read for the x-direction:

$$\frac{\partial \alpha_i}{\partial t} + \frac{\partial \alpha_i v_i}{\partial x} = \Gamma_i \tag{1}$$

$$\frac{\partial \alpha_i v_i}{\partial t} + \frac{\partial \alpha_i v_i v_i}{\partial x} = S_i, \tag{2}$$

where Γ_i, S_i denote source terms for volume flux and momentum transfer between the fields. In a typical continuum model, a pressure gradient is included where the pressure is a function of the sound velocity and density of the field.

Further simplification can be obtained by considering the model as a hyperbolic relaxation system where the source terms, accounting for the interactions between the phases and with exogenous forcing terms, drive the various fields asymptotically towards equilibrium at a finite rate. Imposing immediate equilibrium on such processes enables two dynamic equations to be combined to one and consequently allows for simpler models at the possible cost of a reduction in model fidelity (Flåtten and Lund, 2011). In this case we will assume impose immediate equilibrium on the pressure dynamics of all fields, which is equivalent to assuming the phases to be incompressible, essentially making the pressure gradient a non-local exogenous parameter that enters in the source term. The resulting reduction in fidelity is arguably negligible as the pressure dynamics operate on a much faster time-scale than that of the cuttings transport. Hence, we effectively obtain simpler and more tractable model with modest or negligible cost in model fidelity.

With these assumptions, we can obtain the quasi-linear form by expanding (2):

$$\frac{\partial \alpha_i}{\partial t} v_i + \frac{\partial v_i}{\partial t} \alpha_i + \frac{\partial \alpha_i v_i}{\partial x} v_i + \frac{\partial v_i}{\partial x} \alpha_i v_i = S_i, \tag{3}$$

and inserting (1) into (3), which yields the form

$$\frac{\partial}{\partial t} \begin{bmatrix} \alpha_i \\ v_i \end{bmatrix} + \begin{bmatrix} v_i & \alpha_i \\ 0 & v_i \end{bmatrix} \frac{\partial}{\partial x} \begin{bmatrix} \alpha_i \\ v_i \end{bmatrix} = \begin{bmatrix} \Gamma_i \\ \frac{S_i - v_i \Gamma_i}{\alpha_i} \end{bmatrix}, \tag{4}$$

where the transport matrix, characterizing the system (1) and (2), has the double eigenvalue v_i, corresponding to the velocity of the characteristic. Hence, we see that by removing the equation of state by assuming all densities to be constant (in both time and space), one of the equations of the system (1) and (2) becomes superfluous in the sense of conserving the information propagation properties of the system (due to the repeating eigenvalue) and can be removed to simplify the system. Following the formalism of relaxation processes, we will write (1) and (2) as simply

$$\frac{\partial \alpha_i}{\partial t} + \frac{\partial \alpha_i v_i}{\partial x} = \Gamma_i, \tag{5}$$

where the pressure field typically is contained as a gradient within the source term and can be recovered from the relaxed formulation of (2) from

$$S_i = \frac{\partial \alpha_i v_i v_i}{\partial x}. \tag{6}$$

Consequently, we have argued that for cases where the fast distributed pressure waves are not of critical importance (Aarsnes et al., 2016a), and a constant density is assumed (as is often the case in liquid-solid flow), the momentum balance can be assumed static and the relations of continuity for each field is a sufficient representation of the model. A similar approach has for instance been taken by Girolami et al. (2016), who concluded that the hydrodynamic time scale of the fluid flow is by a factor of order 10^6 smaller than the time scale on which evolution of the sediment bed takes place. Hence, from the solids bed point of view, the time rate of change of the fluid equations becomes instantaneous and the time-dependent terms in the equations may be disregarded. The role of the fluid momentum equation is thus reduced to a closure law relating bulk flow properties such as the superficial liquid velocity to shear stress acting on the bed.

2.1. General relations of continuity

We consider in the following a transient, averaged, three layer model of liquid-solids flow in a conduit, as schematically depicted in the top part of Fig. 1. The three layer model postulation is due to Doron and Barnea (1993, 1996) and Doron et al. (1997), which is a steady-state model. These three layers are typically referred to as the homogeneous layer, a moving bed layer, and a stationary bed layer.

Each layer consists of a combination of two components: liquid and solids. This yields a total of six fields for the model. For each field we denote the volume fraction $\alpha_{i,j}$ and velocity $v_{i,j}$, where $i \in \{h, m, b\}$ denote the homogeneous, moving bed and stationary bed layer respectively, while $j \in [s, l]$ denote the component as solid or liquid. The equations of continuity can be written

$$\frac{\partial \alpha_{i,j}}{\partial t} + \frac{\partial \alpha_{i,j} v_{i,j}}{\partial x} = \sum_k \Gamma_j^{k,i}, \tag{7}$$

where $\Gamma_j^{k,i}$ denotes the source term for transfer of component j from layer k to layer i. Written out

$$\frac{\partial \alpha_{h,s}}{\partial t} + \frac{\partial \alpha_{h,s} v_{h,s}}{\partial x} = \Gamma_s^{m,h} \tag{8}$$

$$\frac{\partial \alpha_{h,l}}{\partial t} + \frac{\partial \alpha_{h,l} v_{h,l}}{\partial x} = \Gamma_l^{m,h} + \Gamma_l^{b,h} \tag{9}$$

$$\frac{\partial \alpha_{m,s}}{\partial t} + \frac{\partial \alpha_{m,s} v_{m,s}}{\partial x} = \Gamma_s^{b,m} - \Gamma_s^{m,h} \tag{10}$$

$$\frac{\partial \alpha_{m,l}}{\partial t} + \frac{\partial \alpha_{m,l} v_{m,l}}{\partial x} = \Gamma_l^{b,m} - \Gamma_l^{m,h} \tag{11}$$

$$\frac{\partial \alpha_{b,s}}{\partial t} + \frac{\partial \alpha_{b,s} v_{b,s}}{\partial x} = -\Gamma_s^{b,m} \tag{12}$$

$$\frac{\partial \alpha_{b,l}}{\partial t} + \frac{\partial \alpha_{b,l} v_{b,l}}{\partial x} = -\Gamma_l^{b,m} - \Gamma_l^{b,h}. \tag{13}$$

Following Doron and Barnea (1993), we assume a constant packing density and homogeneous velocity of the layers b, m. By 'packing density' we mean the solid volume fraction of the stationary (typically 0.63 for close random packing of spheres) and moving bed layers (typically between 0.55 and 0.625 for loose random packing of spheres), where the solid particles are in stationary contact or rolling and sliding against each other, respectively. Hence, denoting the packing density C_i, where $i \in \{b, m\}$, we write $\alpha_i = \alpha_{i,s} + \alpha_{i,l}$, such that $\alpha_{i,s} = C_i \alpha_i$. Further, we assume $v_{i,l} = v_{i,s} = v_i$ for $i \in \{b, m\}$. We note that

$$\alpha_{b,l} = 1 - \alpha_m - \alpha_h - \alpha_{b,s}, \tag{14}$$

and, writing $\Gamma^{k,i} \equiv \Gamma_l^{k,i} + \Gamma_s^{k,i}$, we have

$$C_m \Gamma^{m,h} = -\Gamma_s^{h,m}. \tag{15}$$

When $C_b \neq C_m$, by noting that

$$\Gamma_s^{b,m} = -\Gamma_s^{m,b} \Rightarrow C_b \Gamma^{b,m} = -C_m \Gamma^{m,b}, \tag{16}$$

we get an exchange term between layer b and h:

$$\Gamma_l^{b,h} = \Gamma^{b,m} \left(1 - \frac{C_b}{C_m}\right), \tag{17}$$

These relations allows us to represent the volume fraction of the six fields by the three continuity equations

$$\frac{\partial \alpha_{h,s}}{\partial t} + \frac{\partial \alpha_{h,s} v_{h,s}}{\partial x} = -C_m \Gamma^{h,m} \tag{18}$$

$$\frac{\partial \alpha_m}{\partial t} + \frac{\partial \alpha_m v_m}{\partial x} = \Gamma^{h,m} - \Gamma^{m,b} \tag{19}$$

$$\frac{\partial \alpha_b}{\partial t} + \frac{\partial \alpha_b v_b}{\partial x} = \Gamma^{m,b}. \tag{20}$$

An equivalent formulation is

$$\frac{\partial \alpha_{h,s}}{\partial t} + \frac{\partial \alpha_{h,s} v_{h,s}}{\partial x} = -\Gamma_s^{h,m} \tag{21}$$

$$\frac{\partial \alpha_{m,s}}{\partial t} + \frac{\partial \alpha_{m,s} v_m}{\partial x} = \Gamma_s^{h,m} - \Gamma_s^{m,b} \tag{22}$$

$$\frac{\partial \alpha_{b,s}}{\partial t} + \frac{\partial \alpha_{b,s} v_b}{\partial x} = \Gamma_s^{m,b}, \tag{23}$$

where the layer area fractions are obtained from:

$$\alpha_m C_m = \alpha_{m,s} \tag{24}$$

$$\alpha_b C_b = \alpha_{b,s} \tag{25}$$

$$\alpha_h + \alpha_m + \alpha_b = 1. \tag{26}$$

Hence we have demonstrated that the continuity equations of the transient three layer model of solid-liquid flow can be represented as a third order Partial Differential Equation (PDE).

So far, no assumptions have been made on fluid rheology or inclination. However, depending on conditions, the m and/or b layers will not exist (e.g. in very steep and vertical sections), in which case these fields will be empty and the model can be simplified by removing them.

To complete the model for simulation, (21)–(23) must be combined with closure relations of the velocities v_b, v_m, $v_{h,s}$ and the source terms $\Gamma_s^{h,m}, \Gamma_s^{m,b}$, and finally, appropriate boundary conditions should be derived. The closure relations should be derived by combination of first principle considerations and empirical correlations derived from experiments. To comply with the requirements on simplicity and computational speed, it is the role of the closure relations to account for the presence of the drill pipe, and hence the existence of an annular flow field, as well as the role of drill pipe rotation and potential lateral movement.

For the purpose of illustrating how a complete simulation model is obtained, we will in the following sections of this paper choose a set of simple closure relations from the literature and implement the resulting model. We emphasize, however, that a formulation of the form (21)–(23) can accommodate a wide range of closure relations, and in effect enable turning a set of experimental results into a transient model.

To limit the complexity of the following derivation, and to make our illustration more clear, we limit the model to only two layers. Physically, this is valid depending on the flow patterns. For annular solid-liquid flows, higher superficial velocities, and in particular the presence of drill pipe rotation, enhance solid suspension such that the intermediate layer of rolling and sliding particles becomes very small, see e.g. Khatibi et al. (2018), and may be disregarded for the sake of added simplicity and computational speed.

3. Two layer model

In this section we derive the full two-layer model in the context of a wellbore being drilled, where the solids represent cuttings and the liquid represent the drilling mud.

In considering only two layers in the (21)–(23) formulation, we let the m layer be empty; $\alpha_m = 0$, and consequently set $\Gamma_s^{h,m} - \Gamma_s^{m,b} = 0$. Furthermore, we will assume the bed layer b to be stationary, i.e. $v_b = 0$, which is true for a close to horizontal section such that a potential sliding of the bed due to gravity does not occur, and thus obtain

$$\frac{\partial \alpha_{h,s}}{\partial t} + \frac{\partial \alpha_{h,s} v_{h,s}}{\partial x} = \Gamma_s^{b,h} \tag{27}$$

$$\frac{\partial \alpha_{b,s}}{\partial t} = -\Gamma_s^{b,h}, \tag{28}$$

where $x \in [0, L]$ and t are the space and time variables, with $x = 0$ denoting an upstream inlet and $x = L$ a downstream outlet of the considered flow domain, as depicted in Fig. 1. In addition, we have the closure relations

$$\alpha_b C_b = \alpha_{b,s} \tag{29}$$

$$\alpha_{h,l} + \alpha_{h,s} + \alpha_b = 1. \tag{30}$$

This system, (27) and (28), is a second order hyperbolic PDE with a zero eigenvalue associated with (28).

To complete this system, we further require the closure relations for the slip velocity of particles in suspension, $v_{h,s}$, and the erosion-deposition model $\Gamma_s^{b,h}$.

3.1. Boundary condition

Assuming a positive eigenvalue associated with (27), a boundary condition must be specified at the left ($x = 0$) boundary. If the mass-flux of cuttings at the boundary, W_c is known, the cuttings volume fraction can be found from $W_c = Q_{s,\text{inj}} \rho_s = A \alpha_{h,s} \rho_s v_{h,s}$. Here $Q_{s,\text{inj}}$ denotes the volumetric flowrate of solids at the boundary. For the case of $v_{h,l} = v_{h,s}$ (often used for horizontal pipes, see Section 3.2) we have

$$\alpha_{h,s}(x = 0) \equiv \alpha_{s,\text{inj}} = \frac{Q_{s,\text{inj}}}{Q_{s,\text{inj}} + Q_{l,\text{inj}}}, \tag{31}$$

where $Q_{s,\text{inj}}$ and $Q_{l,\text{inj}}$ are the solid and liquid volumetric flow rates, respectively. In a practical setting W_c, and thus $Q_{s,\text{inj}}$, may be readily estimated from the drill bits dimension and rate of penetration (ROP) based on continuity.

3.2. Slip velocity

For transient cuttings transport models, the slip velocity of a cuttings particle, $v_{h,s}$, may be obtained by applying a local equilibrium assumption and hence taking the vector sum of the liquid velocity $v_{h,l}$ and the particles' terminal settling velocity V_S (Cayeux et al., 2014).

$$v_{h,s} = v_{h,l} + V_S, \tag{32}$$

where the particles' terminal settling velocity V_S may be expressed as

$$V_S = -\sqrt{\frac{4}{3} \frac{d_s g \sin\phi(x)}{C_d} \left(\frac{\rho_s}{\rho_l} - 1 \right)}, \tag{33}$$

with g acceleration of gravity, $\phi(x)$ inclination with respect to horizontal, d_s diameter of cuttings particle, and C_d coefficient of drag. Note that the drag coefficient C_d is a function of the particle Reynolds number, which is a function of the fluids apparent viscosity and furthermore depends implicitly on $v_{h,s}$ via V_S. Further note that drilling fluids are typically shear-thinning and thus the apparent viscosity is a function of the shear rate. This is crucial in order to determine the settling velocity correct, because the shear rate of an individual particle is determined by contributions of both the shear of the background flow field at the particles location and the particle-induced shear based on the relative velocity (Busch and Johansen, 2018).

Forces considered in Eq. (32) are gravity, buoyancy, and drag as the usually dominating particle force. Forces not considered are the Basset and Virtual mass force as the rates of change of flow rates and hence velocities are rather small, i.e. we assume local equilibrium. The Saffman (1968, 1965) lift force (which incorporates the Magnus lift force as a second order correction) does not contribute as Eq. (32) only characterizes the x-component, i.e. the component in the direction of flow, and the lift force primarily acts normal to the flow direction for the 1D approach taken. Particle-particle interactions are neglected here as these are expected to only play a minor role in the homogeneous layer.

The liquid velocity is found from the continuity equation, and assuming an incompressible liquid, implying that $A \alpha_{h,l} v_{h,l} = Q_{\text{inj}}$. I.e. we have from the total volumetric flow at the left boundary:

$$v_{h,l} = \frac{(Q_{l,\text{inj}} + Q_{s,\text{inj}})/A}{1 - \alpha_{h,s} - \frac{\alpha_{b,s}}{C_b}} \tag{34}$$

3.3. Erosion-deposition model

The source term $\Gamma_s^{b,h}$ required in Eqs. (27) and (28) is to be described by an adequate erosion-deposition model. As an example, we apply the erosion-deposition model proposed by Charru et al. (2004)

$$\Gamma_s^{b,h} = E - D, \tag{35}$$

where E, D denotes the erosion and deposition rate, respectively. These are given as

$$D = \frac{V_S d_s^2}{a} \alpha_{h,s}, \tag{36}$$

where V_S is the settling velocity given in (33), d_s is the particle diameter and a is a statistically determined constant which can be taken as 15 (Charru et al., 2004). The erosion rate is given as

$$E = \begin{cases} 0, & \alpha_b = 0 \text{ or } \theta < \theta_t \\ 18bV_S(\theta - \theta_t), & \alpha_b > 0 \text{ and } \theta \geq \theta_t \end{cases}, \tag{37}$$

with the non-dimensional Shields number

$$\theta = \frac{\mu\dot{\gamma}}{(\rho_s - \rho_l)d_s g\cos(\phi(x))}, \tag{38}$$

where $\dot{\gamma}$ is the shear rate, and may be taken as proportional to the intrinsically averaged fluid velocity, $v_{h,\,l}$; and μ is the fluid apparent viscosity.

The threshold for particle motion is given by the Shields curve $\theta_t = f(Re_p)$. However, because the relationship $\theta_t = f(Re_p)$ is implicit, an alternative formulation $\theta_t = f(d_*)$ is typically used, for instance $\theta_t = \frac{0.24}{d_*} + 0.055(1 - e^{-0.02d_*})$ (Soulsby, 1997), where d_* is a dimensionless particle diameter. According to Charru et al. (2004), the coefficient b may depend weakly both on the particle Reynolds number and on the number of moving particles. Since the Charru et al. (2004) formulation is purely based on the Stokes settling velocity this seems reasonable. However, in the modeling approach of Charru et al. (2004) it is taken as a constant and is used as a fitting parameter to experimental data.

Utilizing a particular erosion-deposition model may be considered as grey-box modeling, because the erosion-deposition model allows some insight to the dominating physics of the problem. However, if high-quality experimental data is available and/or not all modeling parameter values are known, it is beneficial to transform the utilized erosion-deposition model to a black-box model by introducing appropriately defined correlation parameters. This reduces the number of parameters needed to specify the closure relations and thus simplifies tuning the model. Assuming that the shear rate is proportional to the intrinsically averaged liquid velocity, $v_{h,\,l}$, the source term containing the erosion-deposition-model can be recast to:

$$D = \beta R\alpha_{h,s} \tag{39}$$

$$E = \begin{cases} 0, & \alpha_b = 0 \text{ or } \alpha_l^* < \alpha_{h,l} \\ \frac{\beta}{\alpha_{h,l}}(\alpha_l^* - \alpha_{h,l}), & \alpha_b > 0 \text{ and } \alpha_l^* \geq \alpha_{h,l}. \end{cases} \tag{40}$$

The correlation parameters β, α_l^*, R are given as:

$$\alpha_l^* = \frac{\mu D_H Q_{l,\text{inj}}/A}{(\rho_s - \rho_l)d_s g\cos\left(\phi(x)\right)\theta_t} \tag{41}$$

$$R = \frac{d_s^2}{a}\frac{1}{\theta_t 18b} \tag{42}$$

$$\beta = \theta_t V_S 18b, \tag{43}$$

where α_l^*, R are dimensionless and β has the unit of $[\frac{1}{\text{time}}]$. In defining the deposition and erosion rates as in (39) and (40), we have adopted the mathematical structure of Charru et al. (2004) in specifying these closure relations, but not necessarily the actual parameters. This allows for a more general framework for tuning the model to fit operating conditions and experimental data not directly covered by the work of Charru et al. (2004).

Eqs. (39) and (40) may alternatively be expressed in terms of the states by noting that $\alpha_b = \alpha_{b,s}/C_b$ and $\alpha_{h,s} = 1 - \alpha_b - \alpha_{h,l}$.

We point out that these parameters are dependent on local conditions, in particular α_l^* which is dependent on the exogenous liquid superficial velocity $Q_{l,\,\text{inj}}/A$. As an example, for higher superficial liquid velocities, the flow of the homogenous layer may become turbulent. In addition, for larger particle diameters, the assumption of Stokes flow is incorrect. The utilized closures (Charru et al., 2004) are based on the Stokes settling velocity V_s and the laminar bed shear stress $\mu\dot{\gamma}$ (see Eqs. (36) and (37)). Here, the molecular fluid viscosity μ may be a function of $\dot{\gamma}$ and the shear rate $\dot{\gamma}$ is based on the superficial liquid velocity and the annular geometry. For an adequate handling of turbulence, this formulation has to be improved by e.g. adding a turbulent viscosity to the molecular fluid viscosity using a simple mixing-length approach. However, wellbore flows are typically either laminar or transitional with bulk Reynolds number in the order of 10^2 to 10^3, which also applies to the experiments conducted by Sanchez et al. (1999), which we will later use to validate the model. Hence, we for now keep the laminar formulation knowing that for higher flow rates, low viscous fluids, and larger particle diameters an error might be present. The significance of the correlation parameters as given can be seen from the steady state relations developed in the following section.

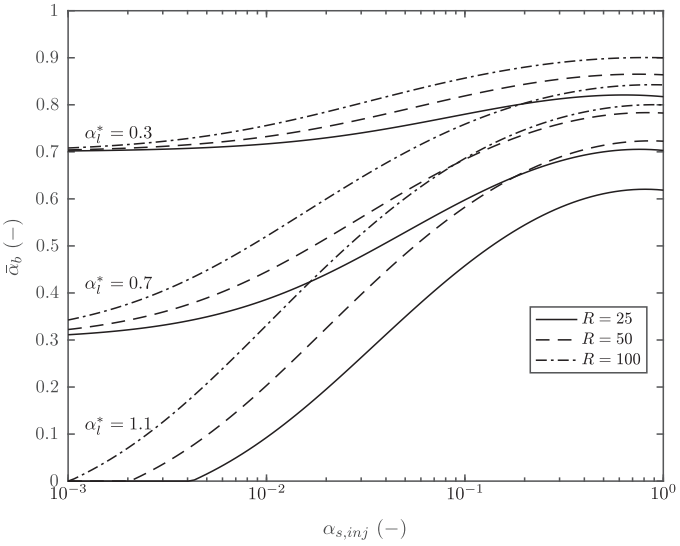

Fig. 2. Effect of correlation parameters R and α_l^* on the steady-state cuttings bed height $\bar{\alpha}_b$.

3.4. Steady state

Denote the steady-state with an overbar. We have, from (27) and (28)

$$\bar{\Gamma}_s^{b,h} = 0 \tag{44}$$

$$\frac{\partial\bar{\alpha}_{h,s}\bar{v}_{h,s}}{\partial x} = 0, \tag{45}$$

which entails

$$\bar{\alpha}_{h,s}\bar{v}_{h,s} = \frac{Q_{s,\text{inj}}}{A}, \tag{46}$$

and using $v_{h,s} = v_{h,l}$:

$$\bar{\alpha}_{h,s} = \frac{Q_{s,\text{inj}}\bar{\alpha}_h}{Q_{s,\text{inj}} + Q_{l,\text{inj}}}. \tag{47}$$

Now, by enforcing $E = D$ (which holds at steady state, see (44)) we obtain:

$$\frac{RQ_{s,\text{inj}}}{Q_{s,\text{inj}} + Q_{l,\text{inj}}}\bar{\alpha}_h + 1 = \frac{\alpha_l^*}{\bar{\alpha}_h}\frac{Q_{l,\text{inj}} + Q_{s,\text{inj}}}{Q_{l,\text{inj}}}, \tag{48}$$

which is a quadratic equation in the state $\bar{\alpha}_h$, i.e.,

$$\bar{\alpha}_h^2 R\frac{Q_{s,\text{inj}}Q_{l,\text{inj}}}{Q_{s,\text{inj}} + Q_{l,\text{inj}}} + \bar{\alpha}_h\frac{Q_{l,\text{inj}}}{Q_{l,\text{inj}} + Q_{s,\text{inj}}} - \alpha_l^* = 0, \tag{49}$$

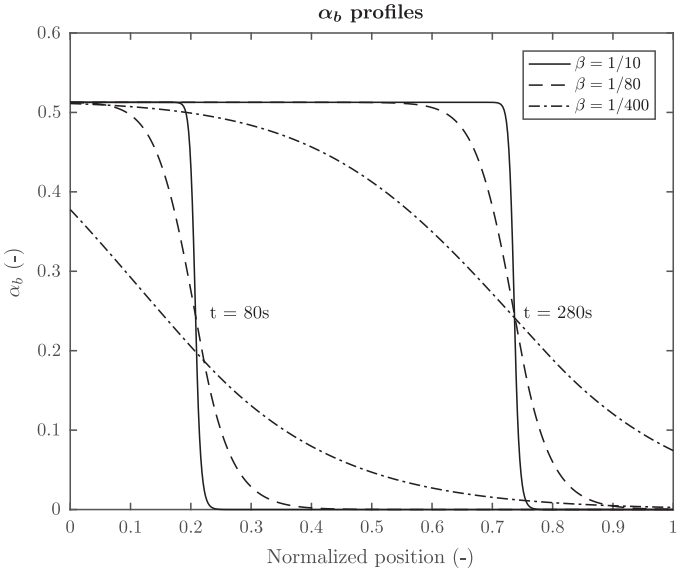

Fig. 3. Effect of changing β on the steepness of the propagating cuttings bed.

hence

$$\bar{\alpha}_h = \frac{Q_{s,\text{inj}} + Q_{l,\text{inj}}}{2RQ_{s,\text{inj}}}\left(-1 + \sqrt{1 + \frac{4R\alpha_l^* Q_{s,\text{inj}}}{Q_{l,\text{inj}}}}\right) \tag{50}$$

and, finally,

$$\bar{\alpha}_b = 1 - \bar{\alpha}_h. \tag{51}$$

Note that using the approximation $\alpha_{s,\text{inj}} \approx \frac{Q_{s,\text{inj}}}{Q_{l,\text{inj}}}$, (50) can be written approximately

$$\bar{\alpha}_h \approx \frac{\alpha_{s,\text{inj}} + 1}{2R\alpha_{s,\text{inj}}}\left(-1 + \sqrt{1 + 4R\alpha_l^* \alpha_{s,\text{inj}}}\right). \tag{52}$$

Relation (52) is shown in Fig. 2. Hence, the steady state cuttings bed is determined by α_l^*, R while the rate of exchange between the cuttings bed and suspension, and consequently the steepness of a propagating cuttings bed, is determined by β as shown in Fig. 3.

3.5. Impact of coefficients

The qualitative effect of the correlation parameters can be summed up as follows.

- α_l^* gives the volume fraction of the liquid flow (essentially the effective cross sectional flow area of the injected liquid relative to the full cross sectional flow area A) at which the threshold Shields number θ_t is achieved. This corresponds to the steady-state liquid flow volume fraction, $\alpha_l^* = \alpha_{h,l}$, when zero solids are injected $Q_{s,\text{inj}} = 0$.
- R determines the deposition rate relative to the erosion rate, and consequently how a non-zero solid injection rate $Q_{s,\text{ inj}} > 0$ affects the steady-state cuttings bed size $\bar{\alpha}_b$.
- β gives the transient rate of exchange between the cuttings in bed and cuttings in suspension.

4. Numerical implementation

The system of equations is discretized in space and time and the partial derivatives resolved with a first order upwind scheme. The discretization is done with the spatial grid size Δx, and temporal step size Δt. We denote the discretized states in parenthesis as $(\cdot)_l^k$ where l is used to denote the discretized position, and k the discretized time, e.g., for $\alpha_{b,\,l}$ we have

$$(\alpha_{b,l})_l^k = \alpha_{b,l}(k\Delta t, l\Delta x). \tag{53}$$

The discretization in space can roughly be understood as a discretization into the computational control volumes depicted in Fig. 1, but this time with a non-zero axial length $\Delta x > 0$.

The first-order upwind discretized version of (27) and (28) can then be written as

$$(\alpha_{h,s})_l^{k+1} = (\alpha_{h,s})_l^k - \frac{\Delta t}{\Delta x}\left((v_{h,s}\alpha_{h,s})_l^k - (v_{h,s}\alpha_{h,s})_{l-1}^k\right) + \Delta t(\Gamma_s^{b,h})_l^k \tag{54}$$

$$(\alpha_{b,s})_l^{k+1} = (\alpha_{b,s})_l^k - \Delta t(\Gamma_s^{b,h})_l^k, \tag{55}$$

with

$$(\Gamma_s^{b,h})_l^k = (E)_l^k - (D)_l^k \tag{56}$$

$$(D)_l^k = \beta R(\alpha_{h,s})_l^k \tag{57}$$

$$(E)_l^k = \begin{cases} 0, & (\alpha_b)_l^k = 0 \text{ or } \alpha_l^* < (\alpha_{h,l})_l^k \\ \frac{\beta}{\alpha_{h,l}}(\alpha_l^* - (\alpha_{h,l})_l^k), & (\alpha_b)_l^k > 0 \text{ and } \alpha_l^* \geq (\alpha_{h,l})_l^k \end{cases} \tag{58}$$

$$(\alpha_{h,l})_l^k = 1 - (\alpha_b)_l^k - (\alpha_{h,s})_l^k, \tag{59}$$

where we are assuming $v_{h,\,s} > 0$.

The boundary condition, (31) is implemented as:

$$(\alpha_{h,s})_0^k = \alpha_{s,\text{inj}}. \tag{60}$$

Table 1
Physical parameters of experiments.

Value	Symbol	Description
0.022 m^2	A	Wellbore model cross-sectional area
2.56–2.64 g/cm^3	ρ_s	Cuttings density
30.48 m	L	Test section length

5. Simulation example

To evaluate the qualitative transient behavior of the model we compare it to the experiments performed by Sanchez et al. (1999). They conducted transient flow loop experiments, where the test section was an almost horizontal annulus with an inner pipe that could be rotated to replicate the conditions of a horizontal section of a wellbore being drilled. Our goal is to show that the presented approach yields an effective transient simulation model for appropriate closure relations, or with a reasonable tuning such as the one utilized in this study. To this end, we tune the correlation coefficients R, α_l^* to achieve the steady-state response from the experiments, and then modify β to match the transient response, to illustrate that the relative simple second order model given by (27) and (28) is sufficient to replicate the transient behavior of the transported cuttings. To be precise: by transient behavior we mean the behavior of the model when it is not at steady-state, i.e. when $\frac{\partial \alpha_{h,s}}{\partial t} \neq 0$ or $\frac{\partial \alpha_{b,s}}{\partial t} \neq 0$. Even though in most cases of slurry transport, solid velocities are not equal to averaged liquid velocity, for reasons of simplicity, and since not all relevant parameters required for modeling were disclosed by Sanchez et al. (1999), the solid velocity is set equal to the averaged liquid velocity $v_{h,s} = v_{h,l}$ for all the simulations.

The physical parameters of the experiments are summarized in Table 1, while Imperial to SI unit conversions is given in Table 3. Note that the liquid density used in the experiments was not provided, however, neither is it required as the tuning procedure employed matches the model output at steady-state to measurements from the experiment, and these outputs can be computed without needing the liquid density.

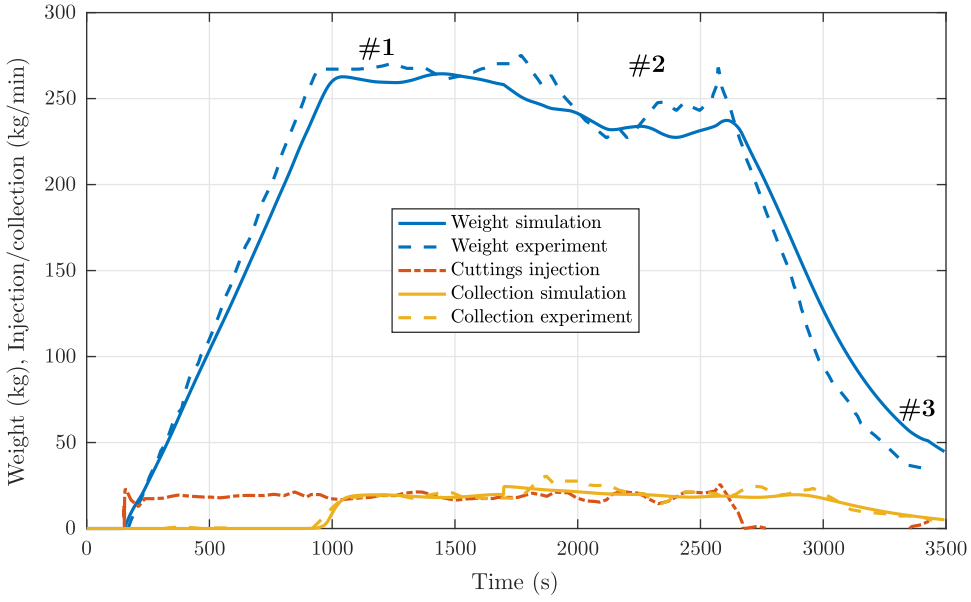

Fig. 4. Trend from experiment 1, with $\phi = 10^\circ$ inclination and 50 RPM pipe rotation starting from $t = 1700$.

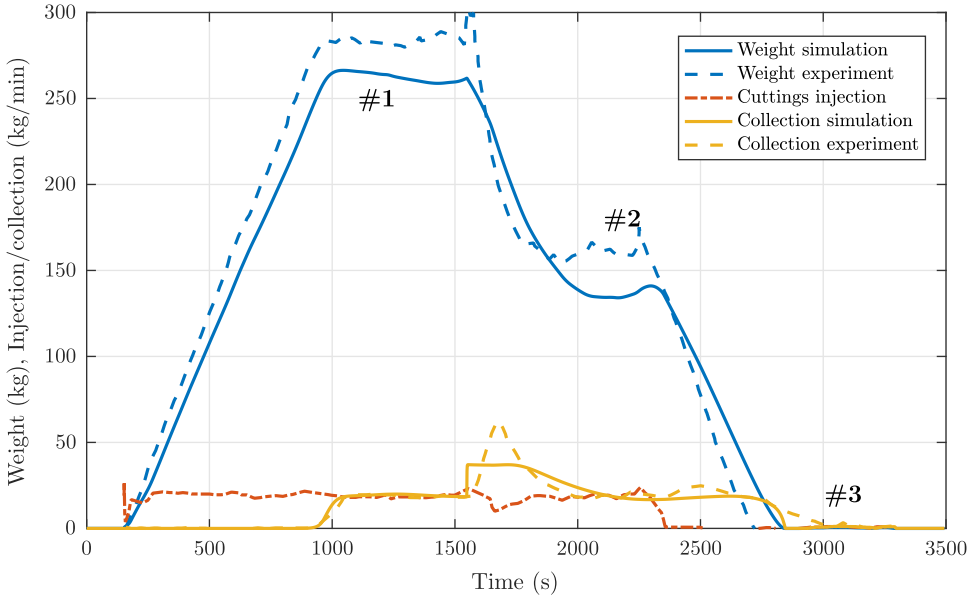

Fig. 5. Trend from experiment 2, with $\phi = 10^\circ$ inclination and 90 RPM pipe rotation starting from $t = 1550$.

5.1. Tuning the correlation coefficients

The measured output of the experiments of Sanchez et al. (1999) is the trend of the mass of the solids in the test section through the experiment. At steady state we have the following relation for the mass of solids in the test section

$$\frac{\text{Mass}}{LA\rho_s} = \bar{\alpha}_{b,s} + \bar{\alpha}_{h,s}, \tag{61}$$

and hence

$$\bar{\alpha}_h = \frac{1}{\frac{Q_{s,\text{inj}}}{Q_{s,\text{inj}}+Q_{l,\text{inj}}} - C_b}\left(\frac{\text{Mass}}{LA(\rho_s - \rho_l)} - C_b\right). \tag{62}$$

Then, using the steady state relation (48), we get

$$R = \frac{Q_{s,\text{inj}} + Q_{l,\text{inj}}}{\bar{\alpha}_h Q_{s,\text{inj}}}\left(\frac{\alpha_l^*}{\bar{\alpha}_h}\frac{Q_{l,\text{inj}} + Q_{s,\text{inj}}}{Q_{l,\text{inj}}} - 1\right) \tag{63}$$

or, equivalently,

$$\alpha_l^* = \frac{\bar{\alpha}_h Q_{l,\text{inj}}}{Q_{l,\text{inj}} + Q_{s,\text{inj}}}\left(\frac{RQ_{s,\text{inj}}}{Q_{s,\text{inj}} + Q_{l,\text{inj}}}\bar{\alpha}_h + 1\right). \tag{64}$$

The particular values used to find the numerical values of the correlation parameters determining the steady-state R, α_l^*, are summarized in Table 2.

5.2. Comments on comparison with experiment

The experimental results of Sanchez et al. (1999) and the simulation results are shown in Figs. 4–9. The steady states from these figures have been noted, summarized in Table 2, and then, using relations (62) and (63), the correlation coefficients R, α_l^* have been found such that the steady state of the simulation model yields a reasonable match to that of the experiment.

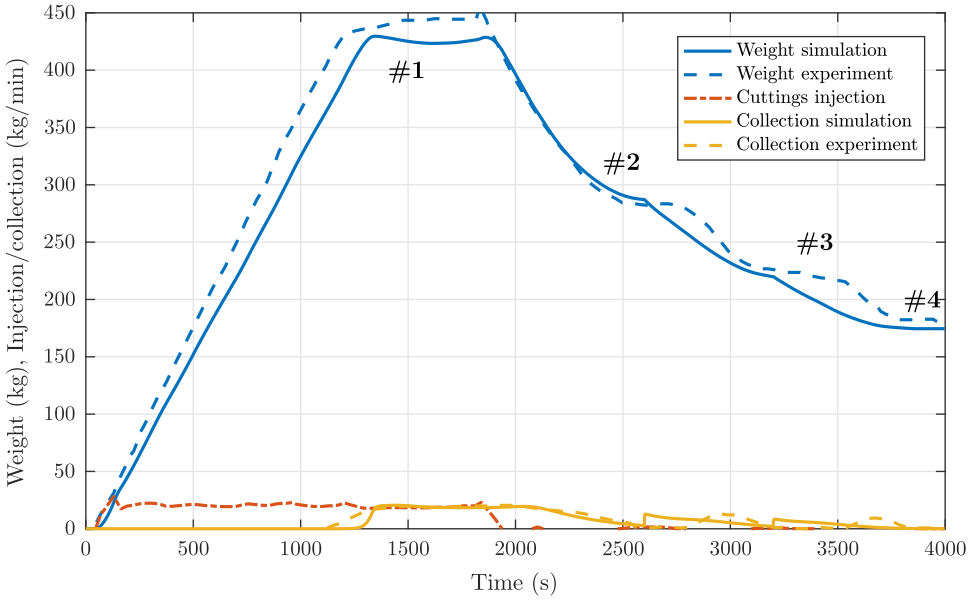

Fig. 6. Trend from experiment 3, with $\phi = 25^\circ$ inclination and 50 RPM pipe rotation starting from $t = 1550$, 50 RPM pipe rotation starting from $t = 2600$, 75 RPM pipe rotation starting from $t = 3200$.

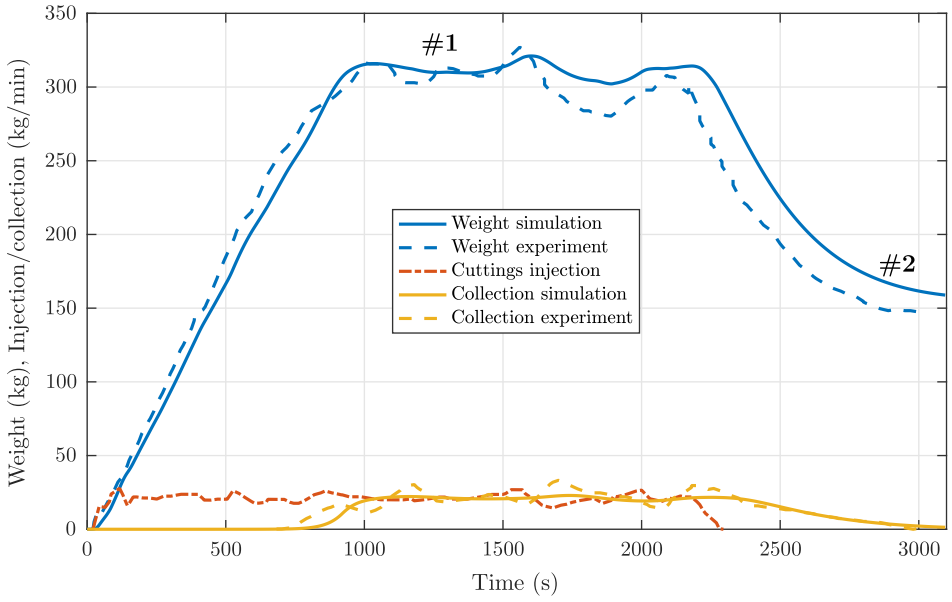

Fig. 7. Trend from experiment 4, with $\phi = 25^\circ$ inclination and 125 RPM pipe rotation.

Table 2
Non-dimensional parameter tuning values.

Ex.	Steady-state #	$Q_{s,\,\mathrm{inj}}/A$	$Q_{l,\,\mathrm{inj}}/A$	$\alpha_{s,\,\mathrm{inj}}$	Mass	$\tilde{\alpha}_b$	R	α_l^*	β
1	#1	0.0064 m/s	1.00 m/s	0.0063	270 kg	0.384	78	0.925	1/50
	#2	–"–	–"–	–"–	245 kg	0.349	–"–	0.980	–"–
	#3	0 m/s	–"–	0	36 kg	0.051	–"–	–"–	–"–
2	#1	0.0064 m/s	1.00 m/s	0.0063	281 kg	0.312	78	0.925	1/50
	#2	–"–	–"–	–"–	164 kg	0.176	–"–	1.152	–"–
	#3	0 m/s	–"–	0	0 kg	0.0	–"–	–"–	–"–
3	#1	0.007 m/s	0.85 m/s	0.0081	445 kg	0.500	90	0.679	1/50
	#2	0 m/s	–"–	0	281 kg	0.321	–"–	–"–	–"–
	#3	–"–	–"–	–"–	218 kg	0.248	54	0.752	–"–
	#4	–"–	–"–	–"–	181 kg	0.207	36	0.793	–"–
4	#1	0.0053 m/s	0.85 m/s	0.0062	295 kg	0.384	54	0.819	1/100
	#2	0 m/s	–"–	0	159 kg	0.349	–"–	–"–	–"–
5	#1	0.0067 m/s	0.85 m/s	0.0078	168 kg	0.179	29	0.969	1/30
	#2	0 m/s	–"–	0	27 kg	0.031	–"–	–"–	–"–
6	#1	0.0055 m/s	0.85 m/s	0.0064	182 kg	0.197	41	0.969	1/50
	#2	0 m/s	–"–	0	27 kg	0.031	–"–	–"–	–"–

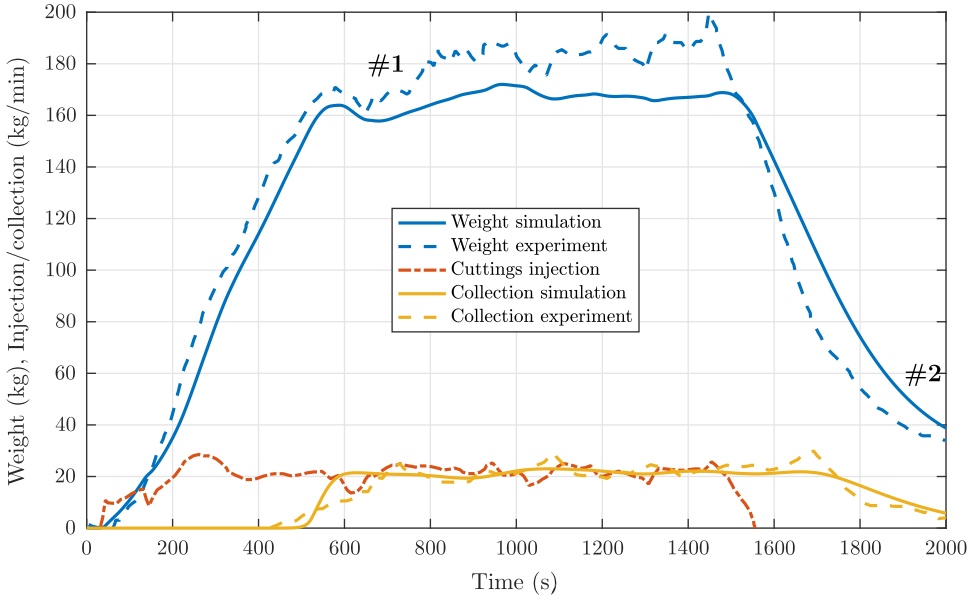

Fig. 8. Trend from experiment 5, with $\phi = 50^\circ$ inclination and no pipe rotation.

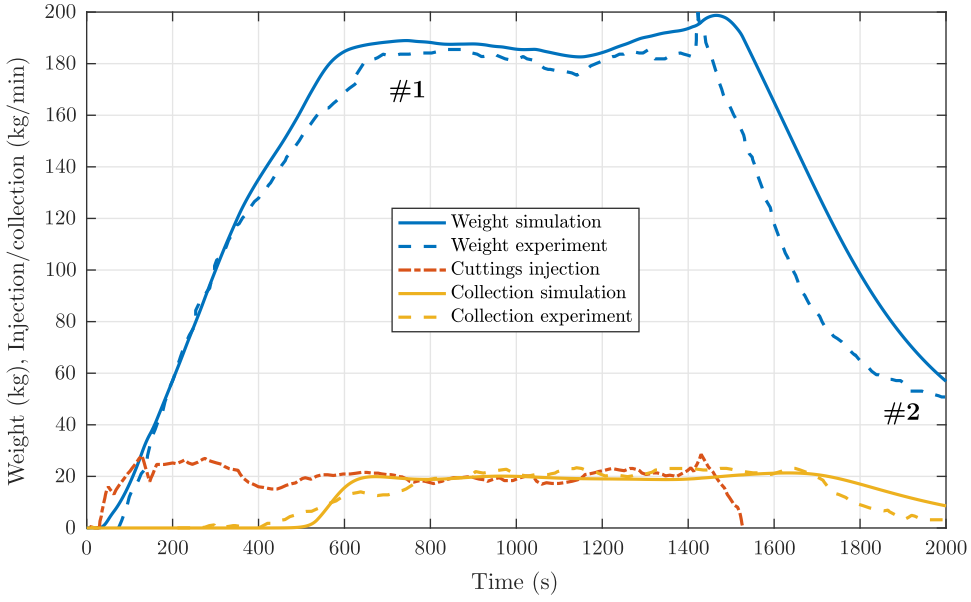

Fig. 9. Trend from experiment 6, with $\phi = 50^\circ$ inclination and 125 RPM pipe rotation.

Table 3
Imperial to SI unit conversions.

US or Imperial	SI units
1 pound (lb)	0.4536 (kg)
1 foot (ft)	0.3048 (m)
1 Gallon per minute (gpm)	6.309×10^{-5} (m^3/s)

For experiment 1, Fig. 4, we first find $\alpha_l^* = 0.980$ for 50 RPM rotation of the drill string from steady-state #3, which corresponds to $Q_{s,\text{inj}} = 0$. Hence we can compute $R = 78$ from steady-state #2, and then assuming R to be constant we find $\alpha_l^* = 0.925$ for the "no rotation" case of steady-state #1. These same values are retained for experiment 2, shown in Fig. 5, where we find $\alpha_l^* = 1.152$ for 90 rpm from steady-state #3. In both these cases, we achieve a good fit in the transient behavior for these experiments with the pipe close to horizontal (note that the 80° specified in Sanchez et al. (1999) is given as angle from vertical, while we use ϕ to denote angle from horizontal).

For experiment 3, Fig. 6 the model fit is less good, although still reasonable. In particular, we note that when pipe rotation is increased there is a delay before cuttings leaves the test section. This could either be an artifact of the test procedure (about which information is somewhat limited), or it could be an actual effect of the specific solid-liquid flow occurring at 25° inclination not accurately captured by the present model.

For the remaining experiments: 4–6, shown in Figs. 7–9, α_l^* is found from steady-state #2 using the fact that $Q_{s,\text{inj}} = 0$, and then R is found from steady-state #1. Here we again see a very good transient fit for the model, even for the steeper inclinations of 50° used in experiment 5 and 6 (Figs. 8 and 9), where the simplifying assumption $v_{h,s} = v_{h,l}$ does not hold and, in addition, bed sliding may occur.

Overall, the model appears to capture the transient dynamics of solid transport in the experiments very well, even without hav-

ing specified information on fluid rheology, pipe eccentricity, pipe rotation rates, or the annular cross-section. This indicates that the approach and the derivation of Section 2 are general and may be applied to scenarios where a transient model of solid transports is required and such specific information is lacking. In particular, the approach is expected to have applications in cuttings monitoring during drilling.

A more powerful model is obtained when the closure relations are specified directly in operating parameters (grey-box model, white-box model), instead of being tuned from data. However, this was not feasible in the present case as the necessary parameters were not provided by Sanchez et al. (1999). Obtaining experimental datasets is highly relevant for modeling activities; however, full disclosure of the related operating parameters is crucial (Busch et al., 2018).

6. Conclusions

The observations from the comparison with experiments in Section 5 lead us towards the conclusion that the simple, coupled, set of transport equations, namely Eqs. (27) and (28), derived from the continuity relations in Section 2, are in many cases sufficient to represent transient mass transport of solids in solid-liquid pipe and annular flow, when used with closure relations which gives accurate steady-state results. This conclusion is valuable in that such a simple dynamic representation of these phenomena makes model implementation and system analysis by simulation much simpler, as well as enabling model-based control and estimation design (Aarsnes et al., 2016b), which in turn can find application to optimize and monitor real-time processes where solid-liquid pipe and annular flow is encountered.

Acknowledgments

The work of the first author was financially supported by ConocoPhillips, AkerBP, Statoil, Wintershall and the RCN grant (203525/O30) DrillWell, by European Unions Seventh Framework Programme for research, technological development and demonstration under Marie Curie grant agreement no [608695], and the FRIPRO Mobility Grant Fellowship Programme (FRICON). The work of the second author was supported by the project Advanced Wellbore Transport Modeling (AdWell). Its sponsor, PETROMAKS 2/the Research Council of Norway (project 228391) and its partners Statoil, Neptune Energy Norge AS, IRIS, UiS, NTNU and SINTEF are gratefully acknowledged for funding and supporting this work.

References

Aarsnes, U.J.F., Ambrus, A., Di Meglio, F., Karimi Vajargah, A., van Oort, E., Aamo, O.M., 2016. A simplified two-Phase flow model using a quasi-equilibrium momentum balance. Int. J. Multiph. Flow 83 (July), 77–85. doi:10.1016/j.ijmultiphaseflow.2016.03.017.

Aarsnes, U.J.F., Flåtten, T., Aamo, O.M., 2016. Review of two-phase flow models for control and estimation. Annu. Rev. Control 42, 50–62. doi:10.1016/j.arcontrol.2016.06.001.

Busch, A., Islam, A., Martins, D.W., Iversen, F.P., Khatibi, M., Johansen, S.T., Time, R.W., Meese, E.A., 2018. Cuttings-transport modeling-Part 1: specification of benchmark parameters with a Norwegian-continental-shelf perspective. In: SPE Drilling & Completion. Society of Petroleum Engineers, Bergen, Norway, pp. 1–32. doi:10.2118/180007-PA.

Busch A., Johansen S.T. An Eulerian-Lagrangian CFD study of a particle settling in an orthogonal shear flow of a shear-thinning, mildly viscoelastic fluid, Journal of Non-Newtonian Rheology (02/2018), In Review.

Busch, A., Khatibi, M., Johansen, S.T., Time, R.W., 2017. A 2D sediment bed morphodynamics model for turbulent, non-Newtonian, particle-loaded flows. In: 12th Int. Conf. CFD Oil Gas, Metall. Process Ind., Trondheim, Norway.

Capecelatro, J., Desjardins, O., 2013. Eulerian-Lagrangian modeling of turbulent liquid-solid slurries in horizontal pipes. Int. J. Multiph. Flow 55, 64–79. doi:10.1016/j.ijmultiphaseflow.2013.04.006.

Cayeux, E., Leulseged, A., Kluge, R., Haga, J., 2016. Use of a transient cuttings transport model in the planning, monitoring and post analysis of complex drilling operations in the North Sea. In: IADC/SPE Drill. Conf. Exhib., Fort Worth doi:10.2118/178862-MS.

Cayeux, E., Mesagan, T., Tanripada, S., Zidan, M., Fjelde, K.K., 2014. Real-time evaluation of hole-cleaning conditions with a transient cuttings-transport model. SPE Drill. Complet. 29 (01), 05–21. doi:10.2118/163492-PA.

Charru, F., Mouilleron, H., Eiff, O., 2004. Erosion and deposition of particles on a bed sheared by a viscous flow. J. Fluid Mech. 519 (2004), 55–80. doi:10.1017/S0022112004001028.

Chien, S.-F., 1994. Settling velocity of irregularly shaped particles. SPE Drill. Complet. 9 (04), 281–289. doi:10.2118/26121-PA.

Doan, Q., Oguztoreli, M., Masuda, Y., Yonezawa, T., Kobayashi, A., Naganawa, S., Kamp, A., 2003. Modeling of transient cuttings transport in underbalanced drilling (UBD). SPE J. 8 (02), 160–170. doi:10.2118/85061-PA.

Doron, P., Barnea, D., 1993. A three-layer model for solid-liquid flow in horizontal pipes. Int. J. Multiph. Flow 19 (6), 1029–1043. doi:10.1016/0301-9322(93)90076-7.

Doron, P., Barnea, D., 1996. Flow pattern maps for solid-liquid flow in pipes. Int. J. Multiph. Flow 22 (2), 273–283. doi:10.1016/0301-9322(95)00071-2.

Doron, P., Simkhis, M., Barnea, D., 1997. Flow of solid-liquid mixtures in inclined pipes. Int. J. Multiph. flow 23 (2), 313–323.

Drew, D.A., 1983. Mathematical modeling of two-phase flow. Ann. Rev. Fluid Mech 15, 261–291.

Flåtten, T., Lund, H., 2011. Relaxation two-phase flow models and the subcharacteristic condition. Math. Model. Methods Appl. Sci. 21 (12), 2379–2407. doi:10.1142/S0218202511005775.

Florence, F., Iversen, F.P., 2010. Real-time models for drilling process automation: equations and applications. In: IADC/SPE Drill. Conf. Exhib.. Society of Petroleum Engineers doi:10.2118/128958-MS.

Girolami, L., Sherwood, J.D., Charru, F., 2016. Dynamics of a slowly-varying sand bed in a circular pipe. Int. J. Multiph. Flow 81, 113–129. doi:10.1016/j.ijmultiphaseflow.2016.02.007.

Kaushal, D., Thinglas, T., Tomita, Y., Kuchii, S., Tsukamoto, H., 2012. CFD modeling for pipeline flow of fine particles at high concentration. Int. J. Multiph. Flow 43, 85–100. doi:10.1016/j.ijmultiphaseflow.2012.03.005.

Khatibi, M., Time, R.W., Shaibu, R., 2018. Dynamical feature of particle dunes in Newtonian and shear-thinning flows: relevance to hole-cleaning in pipe and annulus. Int. J. Multiph. Flow 99 (October), 284–293. doi:10.1016/j.ijmultiphaseflow.2017.10.015.

Larsen, T., Pilehvari, A., Azar, J., 1997. Development of a new cuttings-transport model for high-angle Wellbores including horizontal wells. SPE Drill. Complet. 12 (June), 129–135. doi:10.2118/25872-PA.

Larsen, T.I.F., 1990. A Study of the Critical Fluid Velocity in Cuttings Transport for Inclined Wellbores. University of Tulsa Ph.D. thesis.

Li, J., Luft, B., 2014. Overview solids transport study and application in oil-gas industry-theoretical work. In: Int. Pet. Technol. Conf. International Petroleum Technology Conference doi:10.2523/IPTC-17832-MS.

Li, J., Walker, S., 2001. Sensitivity analysis of hole cleaning parameters in directional wells. SPE J. 6 (04), 356–363. doi:10.2118/74710-PA.

Martins, A., Santana, M., Gaspari, E., Campos, W., 1998. Evaluating the transport of solids generated by shale instabilities in ERW drilling. SPE Int. Conf. Horiz. Well Technol. (December) 254–259. doi:10.2118/50380-MS.

Naganawa, S., Sato, R., Ishikawa, M., 2017. Cuttings-transport simulation combined with large-scale-flow-loop experimental results and logging-while-drilling data for hole-cleaning evaluation in directional drilling. SPE Drill. Complet. 32 (03), 194–207. doi:10.2118/171740-PA.

Peker, S.M., Helvaci, S.S., 2008. Solid-Liquid Two Phase Flow, first ed. Elsevier, Boston. https://www.elsevier.com/books/solid-liquid-two-phase-flow/peker/978-0-444-52237-5.

Philip, Z., Sharma, M.M., Chenevert, M.E., 1998. The role of Taylor vortices in the transport of drill cuttings. In: SPE India Oil Gas Conf. Exhib. Society of Petroleum Engineers, pp. 7–9. doi:10.2118/39504-MS.

Pilehvari, A., Azar, J., Shirazi, S., 1999. State-of-the-art cuttings transport in horizontal wellbores. SPE Drill. Complet. 14 (03), 196–200. doi:10.2118/57716-PA.

Ramadan, A., Skalle, P., Saasen, A., 2005. Application of a three-layer modeling approach for solids transport in horizontal and inclined channels. Chem. Eng. Sci. 60 (10), 2557–2570. doi:10.1016/j.ces.2004.12.011.

Saffman, P.G., 1965. The lift on a small sphere in a slow shear flow. J. Fluid Mech. 22, 385––400. doi:10.1017/S0022112065000824.

Saffman, P.G., 1968. The lift on a small sphere in a slow shear flow - corrigendum. J. Fluid Mech. 31 (3), 624. doi:10.1017/S0022112068999990.

Salazar-Mendoza, R., Espinosa-Paredes, G., 2009. A three-Region hydraulic model for solid-Liquid flow with a stationary bed in horizontal wellbores. Pet. Sci. Technol. 27 (10), 1033–1043. doi:10.1080/10916460802455905.

Sanchez, R.A., Azar, J.J., Bassal, A.A., Martins, A.L., 1999. Effect of drillpipe rotation on hole cleaning during directional-Well drilling. SPE J. 4 (02), 101–108. doi:10.2118/56406-PA.

Soulsby, R., 1997. Dynamics of marine sands: a manual for practical applications. Thomas Telford.

Tomren, P., Iyoho, A., Azar, J., 1986. Experimental study of cuttings transport in directional wells. SPE Drill. Eng. 1 (01), 43–56. doi:10.2118/12123-PA.

Wang, Z., Zhai, Y., Hao, X., Guo, X., Sun, L., 2010. Numerical simulation on three layer dynamic cutting transport model and its application on extended reach drilling. In: IADC/SPE Asia Pacific Drill. Technol. Conf. Exhib. Society of Petroleum Engineers, pp. 1–10. doi:10.2118/134306-MS.

Zhang, F., Filippov, A., Jia, X., Lu, J., Khoriakov, V., 2016. Transient solid-liquid two-phase flow modelling and its application in real-time drilling simulations. In: BHR Gr. - 10th North Am. Conf. Multiph. Technol. 2016, pp. 17–32.